Integration of biomass-fueled power plant and MCFC-cryogenic CO_2 separation unit for low-carbon power production: Thermodynamic and exergoeconomic comparative analysis

Ehsan Akrami [a], Mohammad Ameri [a,*], Matteo V. Rocco [b]

[a] *Faculty of Mechanical and Energy Eng., Shahid Beheshti University, Tehran, Iran.*

[b] *Politecnico di Milano, Department of Energy, via Lambruschini 4, Milan, Italy.*

[*]Corresponding author

E-mail address: m_ameri@sbu.ac.ir

Abstract

Bio-Energy with Carbon Capture and Storage (BECCS) system is emerging as a promising technology to support the development of low carbon power systems. In this context, the present research proposes two scenarios to obtain a biomass-fueled power plant with limited CO_2 emissions. A novel combination of a downdraft gasifier (DG), internally fired gas turbine, molten carbonate fuel cell (MCFC), organic Rankine cycle (ORC), and cryogenic separation unit, is proposed (named scenario 1) and it is compared to a system in which a bottoming steam cycle (SBC) was used instead of the ORC (named scenario 2). To have a deeper insight into the performance of the integrations, a sensitivity analysis and comparative study have been developed in this research in terms of their thermodynamic and economic performance. Sensitivity analysis explores the effects of significant variables on the proposed system performance: fuel cell current density, fuel cell steam to carbon ratio, gas turbine inlet temperature, and CO_2 and fuel utilization factors.

Exergy and exergoeconomic analyses reveal that the air-preheater in scenario 1 and gasifier in scenario 2 are identified as the component with maximum exergy destruction rate (21% and 14% of total respectively) and HRU in scenario 1 and SBC condenser have the lowest value of the exergoeconomic factor (3.76% and 0.01% respectively) due to high thermodynamic inefficiencies, while MCFC in both scenarios has the highest exergoeconomic factor 87.29% and 80.67% respectively due to its high

investment cost. Also, scenario 1 achieves the amount of 83.86 (USD/MW_eh) for LCOE that is 55.76 (USD/MW_eh) more than the reference case and 3.55 (USD/MW_eh) less than the scenario 2.

Keywords

Exergy analysis; exergoeconomic analysis; Municipal Solid Waste; Bio-Energy with Carbon Capture and Storage; Molten Carbonate Fuel Cell; Waste to Energy.

1. Introduction

According to IEA, the World total primary energy demand in 2018 was 14.3 Gtoe, 81% of which was supplied by fossil fuels. Primary energy supplying the power sector reached 38% of the total demand, and yet the significant share was covered by fossil fuels (72%). In the power sector, coal is the predominant source of energy, counting for almost 45% of the energy supply. The power sector dependency on fossil fuels is also reflected in the electricity mix. Moreover, coal and natural gas result in producing respectively 38% and 23% of the global electricity. On the other hand, renewables cover a non-negligible share of the mix, which is equal to 26% [1]. The role of fossil fuels in modern societies is one of the main sources of global CO_2 emissions, as reported mainly by IPCC [2]. In this regard, scientists and policymakers are investigating alternative sustainable pathways to displace fossil fuels from the power industry, proposing innovative hybrid power technologies to support the transition towards a decarbonized society. To this end, solutions proposed so far are diversified, and usually a combination of technical solutions and policy tools [3,4], capable of avoiding possible negative impacts in terms of employment rates and economy feedback caused by such disruptive paradigm change, as underlined by Oei et al. [5].

1.1.Literature review

The technical solutions proposed so far for energy transition can be classified into three main strategies: (i) utilization of renewable energy resources, (ii) implementing low-carbon and carbon-capture and storage technologies, and (iii) exploitation of waste-to-energy systems [3].

Bioenergy is one abundant source of renewable energy in the world, accounting for approximately 13% of the world's energy supply. The share of the traditional use of bioenergy in developed countries (for heating and cooking needs) is around 8%, and the share of modern use is approximately equal to 5% [6].

According to IEA, the use of biomass to generate electricity has increased steadily in the past years, currently accounts for 11% of the world's electricity generation.

Biomass is generally characterized by a high volume and a low heating value: therefore, it is necessary to increase its energy density to make such fuels adequate to be used for electrical power generation. Two methods are adopted for such purpose: (1) biogas production by landfill and (2) syngas production using proper gasifier [7]. The thermochemical gasification process was confirmed as a sustainable management system of Municipal Solid Waste (MSW) by many studies [8–11]. Although the lower heating value of biogas is higher than syngas [12], the use of syngas has several benefits: it is usually produced at high-temperatures and high energy efficiency, causing a significant decrease in volume (80-90%) and mass of biomass (70-80%). In the case of MSW gasification, the minimal area is then required for residual landfilling, and reduction of GHG emissions is also caused by preventing the spread of anaerobic decompositions [13]. Furthermore, in the process of completing the gasification procedure, the selection of the gasification agent has an essential role in the heating value of the produced syngas. The lower nitrogen content agent leads to a higher heating value syngas[13]. Air, O_2 enriched-air, and pure oxygen are the most commonly used agents. Among the available cases, pure oxygen is the most suitable agent for achieving high heating value syngas and low-vitreous ash production. The only deterrent of its use is the high cost of production or purchase, which is justified for gas-fired power plants with a capacity above 100kt/year [13].

In order to provide a consistent definition and sizing of power systems based on Bio-Energy with Carbon Capture and Storage (BECCS), it is essential to define the power generation technology coupled with it: internally and externally fired gas turbines can be employed as power production units [14,15]. Meanwhile, many studies have also been done on biomass-fueled power plants [16–19]. The MSW fired power plant is simulated by Guangchao et al. [16] to produce electrical power with near-zero CO_2 emission. They proposed the oxy-combustion technology as the main part of the power plant, and the required oxygen for combustion is supplied by an Air Separation Unit (ASU). For illustrating the advantages of the assumed system, the results were compared with the results of a conventional MSW based power plant that used air for combustion. With the same fuel consumption rate, the optimized power plant produces less power (5.196 MW) compared to the reference case (10.026 MW). It is mainly

due to power consumption by the ASU section and the flue gas processing compression unit. In contrast, carbon dioxide production has been reduced about 96.24%. Yannay et al. [18] evaluated an MSW-based combined cycle based on detailed exergy and exergoeconomic analysis for heat and power production. Techno-economic approach has been applied to determine the best operating conditions like gasifier working temperature and equivalence ratio. They reported that the cost of produced electricity varied between 0.07 and 0.13 USD/kWh according to the operating conditions. This study has been developed for southern Chile's MSW, and the produced electricity price is competitive with Chilean market electric prices (0.12 USD/kWh). In other work, Maria et al. [17] have introduced a hybrid waste to energy plant which is fed by MSW and natural gas (NG). Also, the proposed plant has been investigated from thermodynamic, economic and environmental points of view. It is compared to several existing single-fueled waste-to-energy facilities and other energy sources, including renewable and non-renewable. An energy and environmental analyses have been conducted on the co-gasification of MSW and agricultural biomass for electricity generation by Natarianto et al. [19]. They could reach 5 kW power production with 19.5% energy efficiency at 40% MSW ratio of fuel.

Bhattacharya et al. [20] considered a biomass fuel-based combined cycle power plant and performed a comprehensive thermodynamic analysis. Mondal et al. developed a comprehensive environmental and economic analysis in two parts for a small-scale combined cycle power plant [21,22]. The proposed plant was comprised of a downdraft gasifier, directly fired gas turbine, and steam bottoming cycle. In comparison, they have declared that the pressure ratio of 8 and TIT of 1100 °C are the optimal conditions for the gas turbine section. The authors investigated the proposed system and reported the overall energy efficiency, the Unit Cost Of Electricity (UCOE), and the specific CO_2 emission to be 43.40%, 0.09 USD/kWh, and 0.77 kg/kWh, respectively.

Carbon Capture and Storage (CCS) technologies can also be included within the BECCS framework, allowing to prevent 90% of CO_2 emissions from power generation plants and industrial processes [23]. Since electrical power is required for the use of these technologies, it is necessary to apply a power generating unit next to the main power plant. Molten Carbonate Fuel cell (MCFC) is indicated as the most suitable technology for this purpose. In addition to power generation, the separation of CO_2 from power plant exhausts gases in its cathode side, which is the second relevant capability of MCFC. Consequently,

extensive studies have been performed on high-temperature fuel cells due to their importance and the possibility of their integration with different types of energy systems [24–29].

An energy and environmental comparison study have been conducted on the utilization of the MCFC-based CO_2 capture and conventional MEA method by Carapellucci et al. [25]. They proposed a 250 MW coal-fired steam plant as a power generation unit. Two scenarios were predicted for the MCFC part: (case 1) The use of extracted steam for fuel cell cathode inlet and feeding its outlet into an oxy-combustion chamber, (case 2) The steam generation by heat exchangers that obtain their heat from the fuel cell. This steam has been injected into the fuel cell anode inlet. The use of conventional MEA is another scenario for carbon dioxide capture (case 3). The simulation results of these three modes were compared with the base mode conditions. Under the specified condition, the overall energy efficiency is equal to 38.40% (base case), 40.15% (case 1), 40.21% (case 2), and 27.12% (case 3). Also, the specific CO_2 emission is equal to 855.20 kg_{CO2}/MW_eh (base case), 54.24 kg_{CO2}/MW_eh (case 1), 54.12 kg_{CO2}/MW_eh (case 2), and 116.28 kg_{CO2}/MW_eh (case 3).

Liqiang Duan et al. [30] evaluated a combined cycle power plant incorporated with CO_2 capture technology and molten carbonate fuel cell technology based on detailed thermodynamic simulations. It was indicated from the results of the modeling that despite the addition of CO_2 technology, the overall system energy efficiency has not changed concerning the initial state of the combined cycle power plant. However, 45% of the carbon dioxide was captured from the power plant. If this rate increases to 85 %, the results show that only 0.67% of the overall system efficiency will be reduced, and it will be equal to 54.96%.

1.2.Work objective

In previously published researches, we deepened MSW-based power plants, MCFC, and WtE technologies [31–33]. Thus, biomass-based power plants, high-temperature fuel cells, CCS technologies, and WtE alternatives have been evaluated independently. Presenting an energy system based on MSW in the context of BECCS, and utilizing a molten carbonate fuel cell as both a carbon capture technology and a power generation unit, is the primary motivation of this work compared to other ones. In this study, a detailed analysis of alternative operational scenarios for an energy system based on MSW-fuel

integrated with MCFC, WtE technology, and the CO_2 separation unit is performed. This study quantifies the thermodynamic and economic performance of the system based on exergy and exergoeconomic analyses. Besides the simulation and analysis of an innovative integrated energy conversion system, a sensitivity analysis has carried out to determine the influence of most relevant design parameters on the operative conditions and the system's performance. Moreover, this study provides an in-depth exergoeconomic analysis to determine the thermodynamic relevance of exergy destructions within plant components, identifying possible strategies for design improvements.

This work is articulated in two parts: first, two feasible design configurations are proposed for the BECCS integrated system (named scenarios 1 and 2), and the related thermodynamic models setup based on literature data. Secondly, the two scenarios are analyzed based on exergy and exergoeconomic analyses, and sensitivity on the main parameters performed.

2. Plant description

The schematic layout of the proposed system configuration is illustrated in Fig. 1, which includes all the main components of the analyzed BECCS integrated system. At the same time, Fig. 2 provides the detailed schemes of the analyzed system configurations (namely, scenarios 1 and 2), which differ based on the structure of the energy conversion unit.

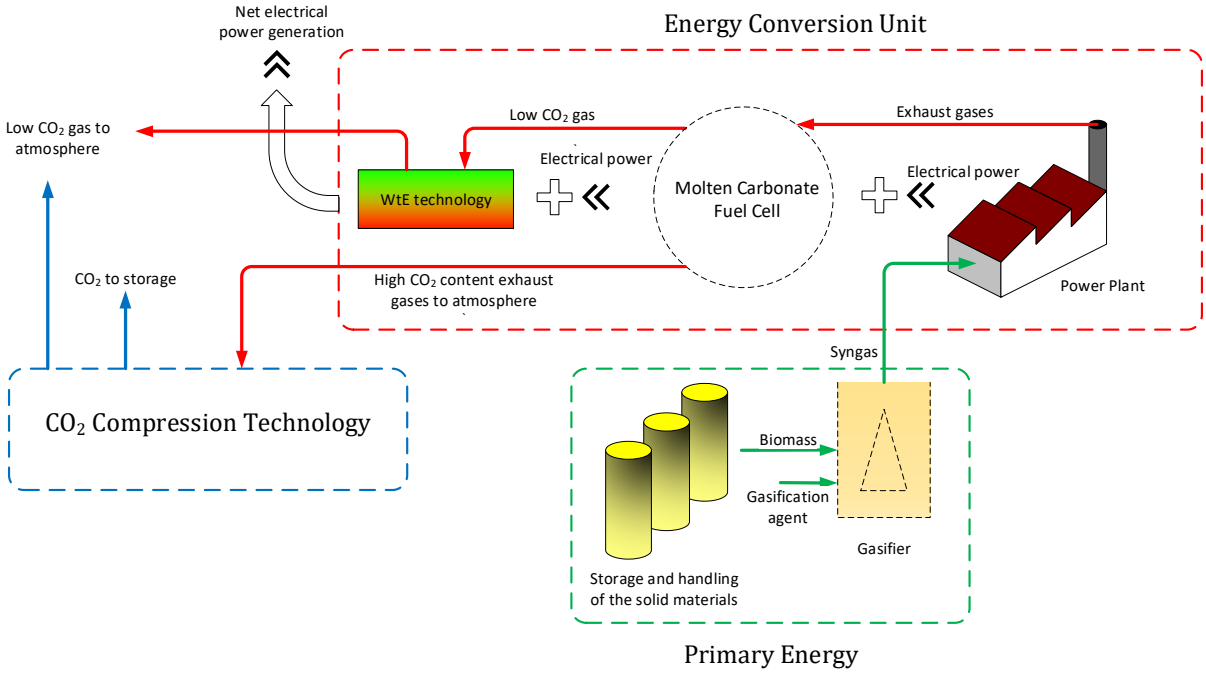

Fig. 1. The layout of the analyzed BECCS system.

Fig. 2a provides a detailed scheme for scenario 1 (also, we assumed MSW-based internally fired gas turbine section as the reference case). MSW is directed to a downdraft gasifier, and oxygen is used as a gasification agent. The produced syngas is directed into the combustion chamber of the internally fired gas turbine, and the combustion is completed by compressed air produced by an air compressor. Then, the exhaust gases from the combustion chamber in the turbine inlet temperature (TIT) feed a gas turbine that generates power. Furthermore, the recovered H_2 and CO from the CO_2 separation and compression section are supplied in the combustion chamber to improve the combustion quality. Then, the exhaust gas from the gas turbine will mix with the preheated air to reach the MCFC operating conditions; notably, CO_2 separation from the gas turbine exhaust gases is the main reason behind the use of MCFC, and its utilization is justified in addition by its significant power production.

The modeling of the given plant requires a set of parameters, which are collected in Table 1. Specifically, the air is preheated to reach the fuel cell's operating temperature: for this purpose, the temperature potential of the exhaust gases from the cathode is used. Since the gas turbine exhaust is directly used to enter the fuel cell cathode section, the required carbonate ions CO_3^{-2} (which produces power by releasing its electrons in transferring the MCFC electrolyte) arises from the exhaust gases from the turbine. By

169 performing this procedure, CO_2 will be separated (according to the fuel cell CO_2 utilization factor), and
170 electricity will be generated. Also, the anode output, where the concentration of CO_2 is high, is partially
171 returned to the anode inlet in proportion to the return ratio. Methane (as fuel) is mixed by the extracted
172 gases and injected into the anode. The rest of the anode outlet stream is transmitted to the self-
173 refrigeration cryogenic separation unit after passing the CC air preheater. The cathode outlet's additional
174 thermal potential is used to generate more electrical power by employing a bottoming Organic Rankine
175 Cycle (ORC). In the last section of the plant, the inlet flow of the cryogenic section must be prepared to
176 enter the compressor, and the water vapor is condensed in a condenser to ensure that no water vapor
177 enters the compressor. Reference [34] has been developed to comprehend how components work and
178 are implemented. In order to complete the cryogenic section and reach the CO_2 saturation temperature
179 and pressure, two sets of heat exchangers have been applied. These heat exchangers have been
180 categorized into the hot and cold heat exchangers. Two drums have also been employed to maximize
181 liquid CO_2 production. To prevent the considerable increase of temperature in the compression process,
182 the inter-cooled compressors were used to provide both the pressure needed to liquefy and avoiding a
183 considerable increase in the temperature. The inlet temperature of drum 1 is a parameter that affects the
184 capacity and the number of components before it. Most of the liquid CO_2 will be separated in the drum 1
185 by decreasing the temperature of this state, and a small portion of gaseous CO_2 will be directed to drum 2
186 with other gases.
187

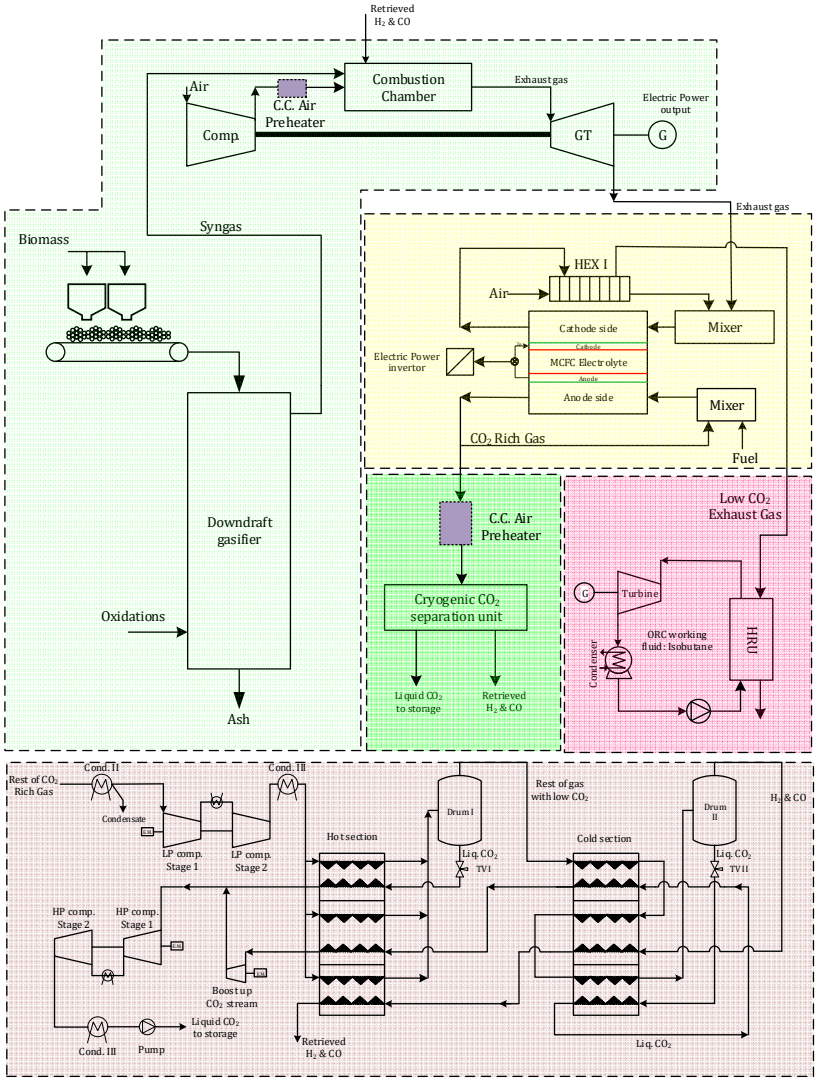

Fig. 2a. Process scheme for scenario 1: combination of DD gasifier, directly fired gas turbine, MCFC, ORC, and cryogenic unit

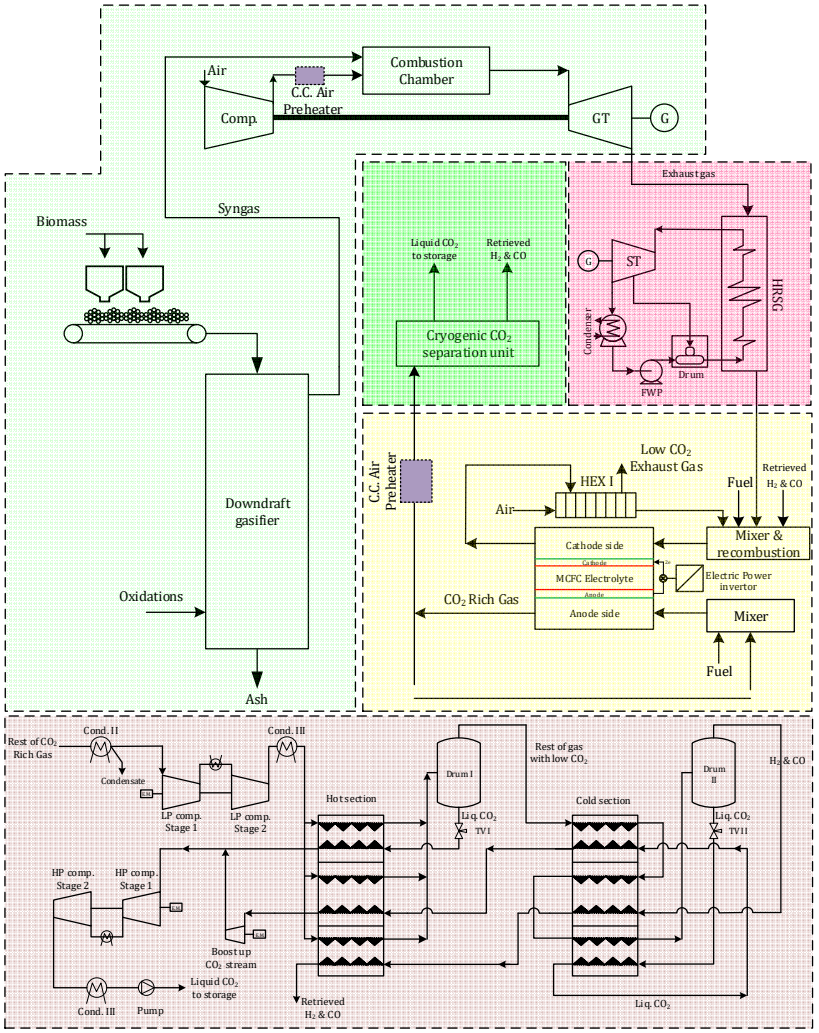

Fig. 2b. Process scheme for scenario 2: combination of DD gasifier, directly fired gas turbine, SBC, MCFC, and cryogenic unit

188

Table 1. Main assumptions adopted for plant simulations

Parameter	value
Gasifier	
MSW mass flow rate	300 ton/day
Gasifier operation temperature [35]	800 °C
Gasification medium [13]	Oxygen
MSW composition [36]	Ultimate analysis and heating value of the Tehran's MSW: 40.5% (C), 3.5% (H), 40.2% (O), 0.8% (N), 15% (Ash), LHV=12.81 (MJ/kg), MC=10%
Directly fired gas turbine	
Pressure levels	1215.6 kPa /101.3 kPa
Maximum temperature [37]	1500 °C
Isentropic efficiency of the compressor and turbine	0.85
MCFC [34]	
Cell current density	1100 (A/m^2)
Fuel utilization factor	0.75
CO_2 utilization factor	0.75
Steam to carbon ratio at anode inlet (r_{SC})	3.5
$T_{cell,anode}$, $T_{cell,cathode}$	650 °C
Fuel cell heat loss to environment (% inlet thermal power)	1%
ΔP cathode and anode streams	2%/3%
ORC	
Working fluid [33]	Isobutane
Pressure levels	2880 kPa /360 kPa
Maximum temperature	140 °C
Isentropic efficiency of ORC turbine	0.85
Hydraulic efficiency of ORC pump	0.9
CO_2 separation and compression [34]	
Minimum temperature	-56 °C
number of LP compressor stages	2
LP compressor inlet temperature	30 °C
number of HP compressor stages	2
HP compressor inlet temperature	24 °C
Liquid CO_2 at pump inlet	10130 kPa, 20 °C
Pump pressure ratio	1.5

189 The positive impact of lower temperature on the downstream processes will cause heavy tasks on the hot
190 heat exchanger section. Furthermore, to minimize the temperature difference in the heat exchanger, the
191 throttle valve must force a high-pressure drop in the passing stream. These opposite effects have led to
192 the selection of -33°C for the drum 1 inlet flow. It should be noted that the choice of this temperature is

193 based on the literature, and the authors have not gone deep into different temperatures [34]. Since the
194 separation of residual CO_2 in the exhaust gases from drum 1 needs another temperature reduction unit,
195 the cold heat exchanger unit is used. The drum 2 inlet temperature is set to be -53°C [38]. The
196 evaporated CO_2 stream, which is heated up by cold and hot heat exchangers, is mixed by liquid CO_2
197 separated by drum 1, and the mixed stream is compressed by the inter-cooled HP compressor. The
198 desired pressure (150 bar) for liquid CO_2 long-range transportation is obtained by a pump. On the other
199 hand, the gas fraction output from drum 2 is heated up in cold and hot heat exchangers and then
200 transmitted to the environment with the least carbon dioxide component.

201 Regarding Fig. 2b, scenario 2 has developed for comparative purposes, intending to recognize whether
202 using a combined cycle power plant or using an organic Rankine cycle along with MCFC and CO_2
203 cryogenic is the most appropriate choice. Since the exhaust gases from the gas turbine have the potential
204 to drive a bottoming steam cycle, they are fed into the HRSG unit to apply this potential to operate a
205 steam cycle. The HRSG provides superheated steam to enter the steam turbine, and its output is directed
206 to the fuel cell inlet section. In addition, the thermal potential of this stream is not enough to enter the fuel
207 cell. For this reason, the additional combustion chamber is employed to increase the temperature up to
208 the fuel cell operating temperature. The fuel for the related combustion will be supplied by recovered H_2
209 and CO and additional natural gas.

210 In addition to the assumptions and numbers considered for some modes of the power plant, other
211 assumptions are applied to the whole plant and will be used in the simulation procedure. These
212 assumptions are as follows:

213 – All the plant components are assumed as operating in steady-state.
214 – Air composition is N_2 (77.48%), O_2 (20.59%), CO_2 (0.03%), and H_2O (1.9%).
215 – Ambient conditions are 101.3 kPa and 25°C.
216 – The MCFC stack operates at a constant temperature.
217 – The gas mixtures are in chemical equilibrium at all points.
218 – All gas mixtures are assumed as the ideal gas.
219

3. Modeling and plant simulation

In this section, the thermodynamic model for the analyzed system is introduced focusing on the main components of the system, namely the downdraft gasifier, the MCFC and other system components.

3.1. Downdraft gasifier

The moisture content in MSW is fed into the downdraft gasifier with oxygen as a gasification agent. The gasification process is a thermochemical endothermic reaction and will result in continuous syngas production, which contains H_2, CO, CO_2, CH_4, H_2O, and N_2 with different mole percentages. The mole and energy balance and the equilibrium ratio between the specified species are used to calculate the composition of the generated gas [39]. The general reaction of the biomass and oxygen is expressed in equation (1): w is for kmol of moisture in kmol of MSW and n_{O_2} is for kmol of oxygen used per kmol of dry MSW and n_i is the coefficient of product i from gasification. Moreover, it is assumed that the biomass composition is moisture free and based on a single carbon atom [40].

$$\boldsymbol{CH_aO_bN_c + wH_2O + n_{O_2}O_2 \rightarrow n_{H_2}H_2 + n_{CO}CO + n_{CO_2}CO_2 + n_{H_2O}H_2O + n_{CH_4}CH_4 + n_{N_2}N_2} \quad (1)$$

The mole balance of C, H, and O are represented by balances of equations 2, 3 and 4.

$$\boldsymbol{n_{CO} + n_{CO_2} + n_{CH_4} = 1} \quad (2)$$

$$\boldsymbol{2n_{H_2} + 2n_{H_2O} + 4n_{CH_4} = 2w + a} \quad (3)$$

$$\boldsymbol{n_{CO} + 2n_{CO_2} + n_{H_2O} = n_{O_2} + b} \quad (4)$$

The reaction equilibrium is modelled based on reactions 5, 6 and 7 according to the literature [39].

$$\boldsymbol{C + 2H_2 \rightleftharpoons CH_4 \;\; ; \Delta H = -41.2\ kJ/mol} \quad (5)$$

$$\boldsymbol{CO + H_2O \rightleftharpoons CO_2 + H_2 \;\; ; \Delta H = -75.0\ kJ/mol} \quad (6)$$

$$\boldsymbol{CH_4 + H_2O \rightleftharpoons CO + 3H_2 \;\; ; \Delta H = -206.2\ kJ/mol} \quad (7)$$

The equilibrium constants governing equations 5, 6 and 7 are defined by equations 8 and 9 [41].

$$\boldsymbol{K_1 = \frac{n_{CH_4}}{n_{H_2}^2}\left(\frac{P/P_0}{n_{tot}}\right)^{-1}} \quad (8)$$

$$\boldsymbol{K_2 = \frac{n_{H_2}n_{CO_2}}{n_{CO}n_{H_2O}}\left(\frac{P/P_0}{n_{tot}}\right)^{0}} \quad (9)$$

The moisture stoichiometric coefficient is determined based on equation 10 as a function of the moisture content (MC) per kmol of biomass derived from Table 1.

$$\boldsymbol{w = \frac{\dot{m}_{biomass} MC}{18(1 - MC)}} \tag{10}$$

Also, the equilibrium constants are evaluated by using the Gibbs function, as reported by equations 11 and 12.

$$-\frac{\boldsymbol{\Delta G_1^0}}{\boldsymbol{\bar{R} T_g}} = \boldsymbol{lnK_1} \tag{11}$$

$$-\frac{\boldsymbol{\Delta G_2^0}}{\boldsymbol{\bar{R} T_g}} = \boldsymbol{lnK_2} \tag{12}$$

Gibbs functions are determined as functions of enthalpy, entropy and gasification temperature T_g based on equations 13 and 14.

$$-\boldsymbol{\Delta G_1^0} = \boldsymbol{\left(\bar{h}_{CH_4} - T_g \bar{s}^0_{CH_4}\right) - 2\left(\bar{h}_{H_2} - T_g \bar{s}^0_{H_2}\right)} \tag{13}$$

$$-\boldsymbol{\Delta G_2^0} = \boldsymbol{\left(\bar{h}_{CO_2} - T_g \bar{s}^0_{CO_2}\right) + \left(\bar{h}_{H_2} - T_g \bar{s}^0_{H_2}\right) - \left(\bar{h}_{CO} - T_g \bar{s}^0_{CO}\right) - \left(\bar{h}_{H_2O} - T_g \bar{s}^0_{H_2O}\right)} \tag{14}$$

Thanks to all the previously introduced equations, the energy balance for the gasifier (equation 15) can be finally solved, where $\bar{h}_f^0$ is the standard enthalpy of formation and the $\bar{h}^0_{f,MSW}$ is the enthalpy formation of MSW. The latter parameter is determined by equation 16 based the method illustrated by Zianal et al. [42], where n_k represents n_{CO_2} and n_{H_2O} and the Higher Heating Value of the MSW HHV_{MSW} is calculated based on equation 17 (C, H, O, N are the mole percentage of the carbon, hydrogen, oxygen and nitrogen which are replaced by ultimate analysis results from Table 1) [43].

$$\begin{aligned}\boldsymbol{\bar{h}^0_{f,MSW} + w \times \bar{h}^0_{f,H_2O} = n_{H_2}\left(\bar{h}^0_{f,H_2} + \Delta\bar{h}^0_{H_2}\right) + n_{H_2O}\left(\bar{h}^0_{f,H_2O} + \Delta\bar{h}^0_{H_2O}\right) + n_{CO}\left(\bar{h}^0_{f,CO} + \Delta\bar{h}^0_{CO}\right)} \\ + n_{CO_2}\left(\bar{h}^0_{f,CO_2} + \Delta\bar{h}^0_{CO_2}\right) + n_{CH_4}\left(\bar{h}^0_{f,CH_4} + \Delta\bar{h}^0_{CH_4}\right) + n_{N_2}\left(\bar{h}^0_{f,N_2} + \Delta\bar{h}^0_{N_2}\right)\end{aligned} \tag{15}$$

$$\boldsymbol{\bar{h}^0_{f,MSW} = HHV_{MSW} + \sum n_k \bar{h}^0_{f,k}} \tag{16}$$

$$\boldsymbol{HHV = 0.3491\, C + 1.1783 H - 0.1034 O - 0.0151 N} \tag{17}$$

3.2. Molten Carbonate Fuel Cell (MCFC)

Based on the literature review, MCFC electrochemical modeling and equations of chemical reactions that occur in its anode and cathode sides are modeled based on the work of Haghighi et al. [44]. Specifically,

the reforming reaction is described by reactions 18 and 19. The equilibrium constant of Water Gas Shift can be calculated from data available in Table 2.

$$CH_4 + H_2O \longrightarrow CO + 3H_2 \quad (18)$$

$$CO + H_2O \longrightarrow CO_2 + H_2 \quad (19)$$

Reaction occurring in the anode and cathode are reported by equations 20 and 21.

$$H_2 + CO_3^{2-} \longrightarrow H_2O + CO_2 + 2e^- \quad (20)$$

$$O_2 + 2CO_2 + 2e^- \longrightarrow 2CO_3^{2-} \quad (21)$$

The electrical output power of MCFC is obtained based on equation 22, where α, V_c, and I are respectively the DC/AC converter coefficient, the fuel cell voltage and the current intensity.

$$W_{MCFC} = \alpha \times V_c \times I \quad (22)$$

The current and current density are determined based on equations 23 and 24 [45], where z, n, s, F and N denote the electronic flow of the reaction, the number of electrons produced per H_2 mole that dissociate through a single electrochemical reaction, the active surface area, Faraday constant and number of batteries, respectively.

$$I = \frac{znF}{N} \quad (23)$$

$$i_c = \frac{I}{s} \quad (24)$$

Cell voltage can be defined based on equations 25 and 26 [45], where V_N is the ideal Nernst voltage and V_{loss} is the voltage losses caused by cathode, anode and ohmic resistance, collected by Table 2.

$$V_c = V_N - V_{loss} \quad (25)$$

$$V_{loss} = (R_{an} + R_{ca} + R_{ohm}) \times i_c \quad (26)$$

Table 2. The electrochemical equations for the MCFC

MCFC voltage terms [24]	
Equations	
Nernst Voltage	The equilibrium constant of the water gas shift reaction at the MCFC cathode side [46]:
$V_N = \frac{\Delta G}{nF} + \frac{RT}{nF} ln\left[\frac{P_{H_2,an}\left(P_{O_2,an}\right)^{\frac{1}{2}} P_{CO_2,ca}}{P_{H_2O,an} \cdot P_{CO_2,an}}\right]$	$K_{WGS} = \exp\left(\left(\frac{4276}{T_{cell}}\right) - 3.961\right)$
$\Delta G = 242000 - 45.8T$	$K_{WGS} = \frac{P_{Co_2} P_{H_2}}{P_{CO} P_{H_2O}}$
	By assuming that x and y are the molar flow

Anode overpotential

$$R_{an} = 2.27\times10^{-9}\times exp\left(\frac{E_{act,an}}{RT}\right)\times {P_{H_2}}^{-0.42}{P_{CO_2}}^{-0.17}{P_{H_2O}}^{-1.0}$$

$$E_{act,an} = 53.5\ \frac{kJ}{mol}$$

Cathode overpotential

$$R_{ca} = 7.505\times10^{-10}\times exp\left(\frac{E_{act,ca}}{RT}\right)\times {P_{O_2}}^{-0.43}{P_{CO_2}}^{-0.09}$$

$$E_{act,ca} = 77.229\ \frac{kJ}{mol}$$

Ohmic resistance

$$R_{ohm} = 0.5\times10^{-4}\times exp\left[3016\left(\frac{1}{T}-\frac{1}{923}\right)\right]$$

rates of CO and H_2, and considering the electrochemical reaction of the water gas shift:

$$K_{WGS} = \frac{(\dot{n}_{CO_2,in,ca}+x+y)(x-y)}{(\dot{n}_{CO,in,ca}-x)(\dot{n}_{H_2O,in,ca}-x+y)}$$

$$y = U_f(\dot{n}_{H_2,in,ca}+x)$$

$$U_f = \frac{\dot{n}_{H_2,in,ca}-\dot{n}_{H_2,out,ca}}{\dot{n}_{H_2,in,ca}}$$

3.3. Other system components

To reduce the gas flow temperature, a self-cooling process has developed for CO_2 separation. The ORC and the SBC sections are described in the previous works of the authors [46,47]: all the mass and energy balance equations which are used for modeling of the cryogenic section, are retrieved in the available literature [47] and are not reported here for the sake of conciseness. The main assumptions for the simulation of these units are collected in Table 1.

4. Exergy and exergoeconomic analysis

In this section, the fundamental equations required for the application of exergy and exergoeconomic analyses are reported. Moreover, parameters such as energy and exergy efficiencies, CO_2 emissions rate, specific cost of products, and exergoeconomic indicators are assessed to provide an in-depth view of the system thermodynamic and economic performance.

Exergy (sometimes named Availability) is defined as the amount of reversible mechanical work that could be extracted from a system by bringing it into physical and chemical equilibrium with the environment and by only interacting with the environment at its temperature [48]. The use of exergy analysis (or availability analysis) emerges since about 1950 [49], and it has brought under the spotlight by several authoritative literature references, the most relevant of which are the publications of Kotas [48], Bejan [50], Moran [47], and other well-known names in the field of thermodynamics. Besides this, exergy has assumed as the

basis for several advanced analysis methods like Thermoeconomic analysis (sometimes referred to as exergoeconomic analysis) by Valero [51] and by Tsatsaronis [52], Cumulative Exergy Consumption by Szargut, Extended Exergy Accountings by Sciubba [53]. Exergoeconomic analysis proved to be a useful method capable to integrate thermodynamic and economic analyses of energy systems, and it has adopted for the purposes of cost assessment and design improvement. According to the literature, the exergy balance can be considered as follows:

$$\dot{Ex}_Q + \sum \dot{m}_i \, ex_i = \dot{Ex}_w + \sum \dot{m}_e \, ex_e + \dot{Ex}_D \tag{27}$$

Where subscripts i and e represents the inlet and outlet flows, respectively [48]. Also, the exergy destruction rate of each system component can be compared to the total exergy destruction rate within the system, defined based on equation 28.

$$y^*_{D,k} = \frac{\dot{Ex}_{D,k}}{\dot{Ex}_{D,tot}} \tag{28}$$

The exergoeconomic analysis is also defined based on exergy balances previously defined by introducing economic cost rate balances defined for each component as in equation 29: given one generic k_{th} component, total cost rates of exiting flows are expressed as the sum of the cost rates associated with the exergy streams entering the analyzed component plus the total cost rate associated with capital investments, operation and maintenance costs $\dot{Z}_k$ [54,55]. The Specific Exergy Costing Method (SPECO, introduced by Lazzaretto and Tsatsaronis [56]) is used in this work for assessing the unit exergy costs of product flows.

$$\dot{C}_{w,k} + \sum \dot{C}_{e,k} = \dot{C}_{q,k} + \sum \dot{C}_{i,k} + \dot{Z}_k \tag{29}$$

The total cost rate of each energy or bulk flow is defined based on equation 30 as a function of specific exergy cost and total exergy of the same flow, as in equation 30.

$$\dot{C}_k = c_k \dot{Ex}_k \tag{30}$$

Total cost rates for investments and O&M ($\dot{Z}_k$) can be calculated based on equation 31 [55], where φ and N are the maintenance factor (set equal to 1.1) and the annual plant operation hours (7446 h) respectively, and the Capital Recovery Factor (CRF) is expressed by equation 32 as a function of the interest rate i_r (12%) and the system lifetime n (20 years).

$$\dot{Z}_k = \frac{Z_k \, CRF \varphi}{N} \tag{31}$$

$$CRF = \frac{i_r(1+i_r)^n}{(1+i_r)^n - 1} \quad (32)$$

The formulations of the cost balances require auxiliary equations and purchased equipment costs for each component of the proposed system [46]. Also, the cost functions of various components in the proposed plant are listed in Table 5 of Appendix A.

Alongside the assessment of the specific costs rates associated to fuels ($c_{F,k}$) and products ($c_{P,k}$) of each system component, quantified based on equations 33 and 34, it is possible to calculate the cost rate of exergy destruction ($\dot{C}_{D,k}$) based on equation 35 by properly handling the exergy and the cost rate balances: the latter expresses the role of thermodynamic irreversibility in increasing the overall product cost rate.

$$\dot{C_{F,k}} = c_{F,k}\dot{Ex}_{F,k} \quad (33)$$

$$\dot{C_{P,k}} = c_{P,k}\dot{Ex}_{P,k} \quad (34)$$

$$\dot{C_{D,k}} = c_{D,k}\dot{Ex}_{D,k} \quad (35)$$

Once all the previous quantities have derived, it is possible to rank all the components of the system based on the sum of cost of exergy destructions $\dot{C_{D,k}}$ and the investment and O&M cost $\dot{Z}_k$ rates in order to identify the most crucial components on which focus the attention in order to increase the economic performance of the overall system. Then, the exergoeconomic factor f_k (36) is useful to compare the relative weight of investment cost and cost of exergy destructions for each component, identifying the best strategy for system optimization, while the relative cost difference r_k (37) reveals the practical margins of improvements in each component.

$$f_k = \frac{\dot{Z}_k}{\dot{Z}_k + \dot{C}_{D,k}} \quad (36)$$

$$r_k = \frac{c_{P,K} - c_{F,K}}{c_{F,K}} \quad (37)$$

5. Results and validation

5.1. Model validation

Software-based simulations are developed by Engineering Equation Solver (EES, http://fchartsoftware.com/ees/) and compared against available results in the literature, especially for the downdraft gasifier and MCFC. [36,45]. Validations of the gas turbine, steam bottoming cycle, and ORC units are available in previous authors' works [33,57]. Also, Simulated results are plotted against the

literature data in Fig. 3. As shown in this figure, there is a good fit between the related results. As the error bars are displayed in Fig. 3, there is a 3% error in the voltage value for the 500 A/m^2 current density. And this value increases up to 12% with increasing current density to 2300 A/m^2. This is due to the molar fraction of the cathode and anode inlet. Because these percentages are effective in calculating fuel cell voltage, according to Eq. (25) and Table 2.

MSE (mean squared error, which is defined in Eq. (39)) has also been measured to ensure the accuracy of simulation results. The calculation revealed that MSE is 0.003 for the seven current density selected values. In the voltage range (0-0.85), the estimated value for MSE confirms our claim to accurate modeling.

$$MSE = \frac{1}{N}\sum_{i=1}^{N}(f_i - y_i)^2 \tag{39}$$

Where N is the number of data points and f_i is the value obtained by the simulation and y_i is the value added by reference data [58].

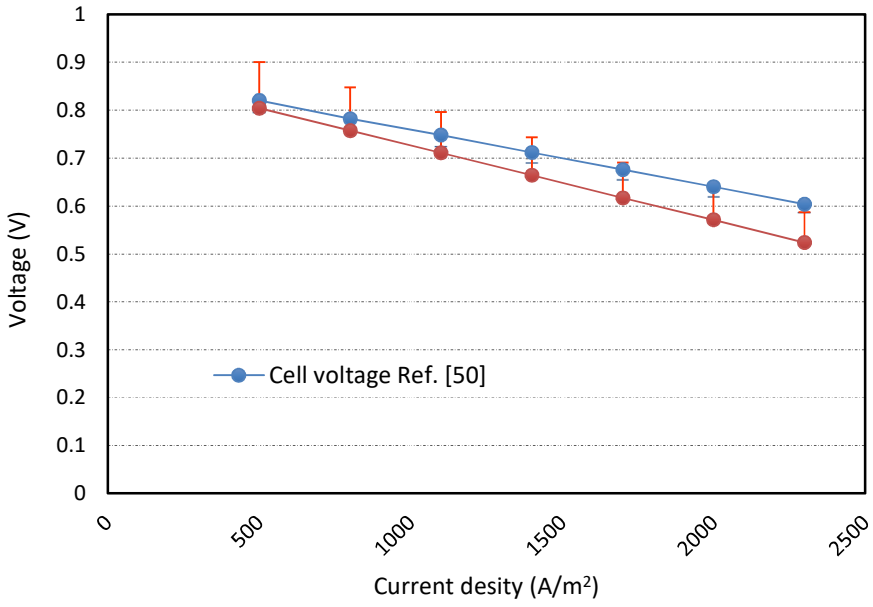

* Main parameters which are adopted in the literature and simulation validation are U_f=75%, U_{CO2}=75%, U_{O2}=11%, r_{SC}=3.5, Total active area=89890 m^2, Cell temperature= 636 °C

Fig. 3. Comparison of the present simulation results with the Campanari et al. [59] results for the MCFC

The results of the downdraft gasifier simulation are then validated. Table 3 compares the results of the simulation with the literature data [41] and the experimental data [59]. The produced syngas components are described on the dry basis, and there is a decent agreement between the results.

Table 3. Validation of the simulated model for downdraft gasifier, O_2 as gasifier medium and m_c=10%

Component (dry basis)	Present study	Ali et al. [41]	Experimental results [59]
H_2	26.86	36.14	32
CO	43.39	47.93	48
CH_4	3.1	3.01	2
CO_2	26.07	12.33	15
N_2	0.6	0.59	3

5.2. Sensitivity analysis

Sensitivity analysis is one of the steps outlined in introduction section. This analysis is very important for the selection of design parameters and has a significant impact on the overall performance of the power plant. Also, in order to be consistent in analyzing the results, the effects of the fuel cell parameter variations are examined for scenario 1, because the variations trends are similar in both scenarios.

One of the units where changing its parameters causes many effects in the simulation results is the fuel cell section. Therefore, variations of parameters such as current density, U_F, U_{CO2}, r_{SC} in sensitivity analysis have been studied.

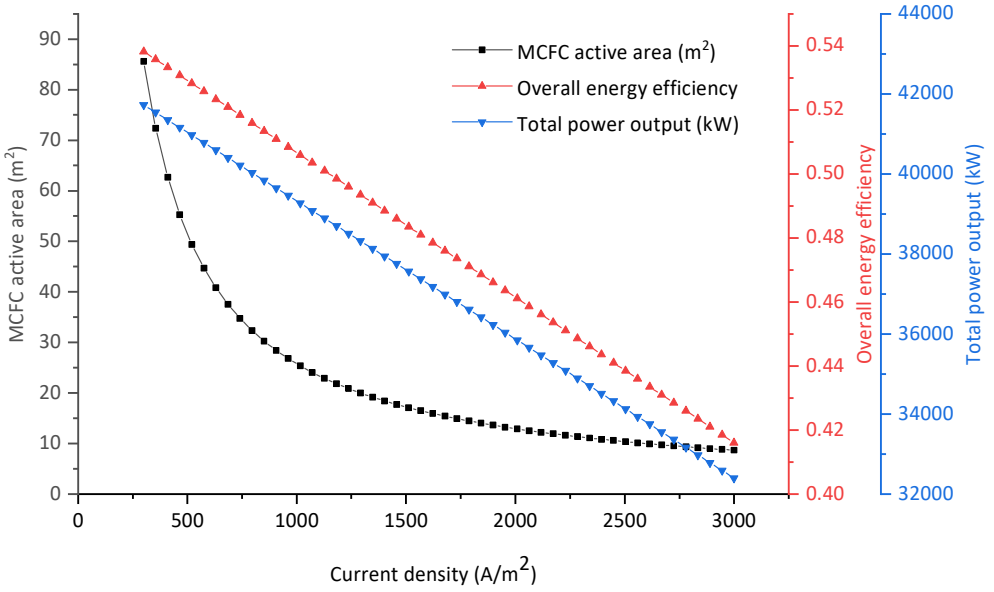

Fig. 4. Influence of the MCFC current density on the total power output and MCFC active area

Fig. 4 reports the variation of the total power generation, energy efficiency (proportional to energy performance), and fuel cell active area (proportional to fuel cell investment cost) as a function of current density. Increasing the current density caused to decrease in the fuel cell voltage, and consequently the fuel cell power generation detracted. Reducing power generation in fuel cells reduces total power generation and energy efficiency. In contrast, increasing the current density has a positive effect on the fuel cell's active area. Lower investment cost of the fuel cell is obtained by reducing the active area. It should be considered that increasing in the current density is limited by the fuel cell operating. Besides, increasing the current density by more than 2000 (A/m^2) does not have a significant effect on the reduction of the active area. Still, it results significantly in the linear reduction trend of the power production and overall energy efficiency.

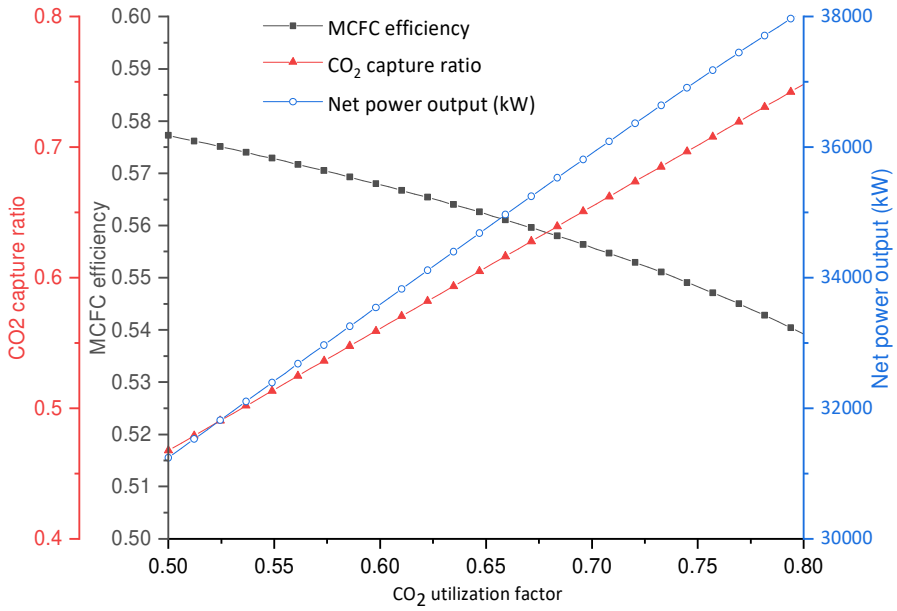

Fig. 5. Influence of the fuel cell CO_2 utilization factor on the total power output, MCFC efficiency, and carbon capture ratio

Fig. 5 shows the effects of CO_2 utilization factor variation on fuel cell efficiency, CO_2 capture ratio, and the net power output. This factor, which relates to CO_2 transmitted from the cathode to the anode section, significantly affect the fuel cell energy balance. The fuel utilization rate and current density are the parameters that are assumed to be constant besides changing this parameter. Also, the cathode inlet stream is not constant and alters by changing the CO_2 utilization factor. As depicted in Fig. 5, the change of U_{CO2} from 0.5 to 0.8 decreases the electrical efficiency of the fuel cell. Although the cathode inlet flow rate is not assumed as a constant parameter, the flow rate of the exhaust gases from the gas turbine is constant, and only the mixed air changes with these flows. In general, the CO_2 molar fraction of the cathode inlet stream is constant and more CO_2 is transported from the fuel cell electrolyte to the anode side by increasing the U_{CO2}. This transmission increases the fuel consumed by the fuel cell. Consequently, MCFC electrical efficiency decreases due to constant U_F. Additionally, the CO_2 capture rate can be expected to be high because of the direct relationship between them. On the other hand, as shown in Fig. 6, and oxygen concentration in the cathode causes an increase in the cathode resistance and consequently reduces the cell voltage due to the increase in U_{CO2}. Increasing in cathode resistance

boosts up the fuel cell temperature, which is assumed to be constant in the simulation. Therefore, with constant temperature and current density, the active area of the fuel cell rises by Increasing the cathode resistance. Finally, the voltage drop rate is lower than the increase rate of the active area, and the MCFC power output will increase beyond the increase of U_{CO2}.

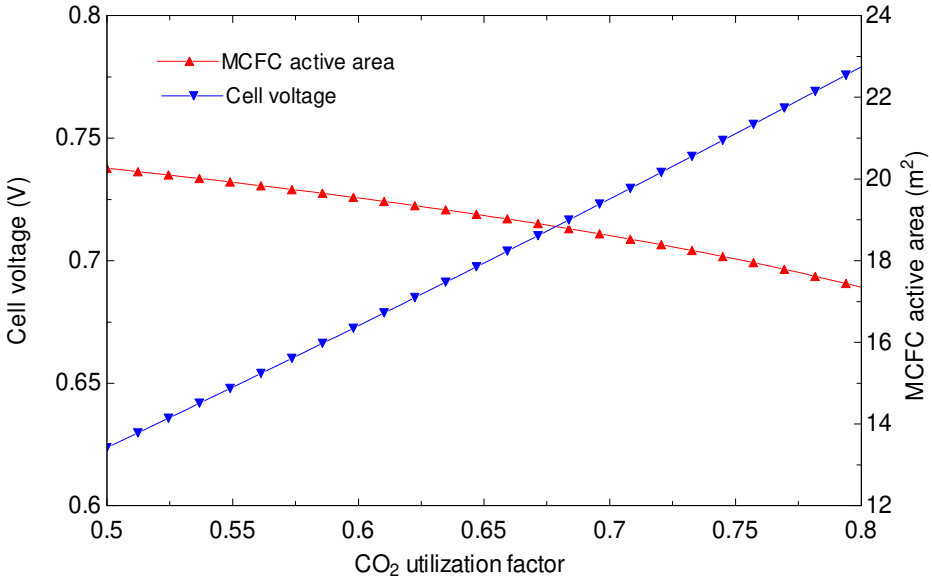

Fig. 6. Influence of the fuel cell CO_2 utilization factor on fuel cell voltage and active area

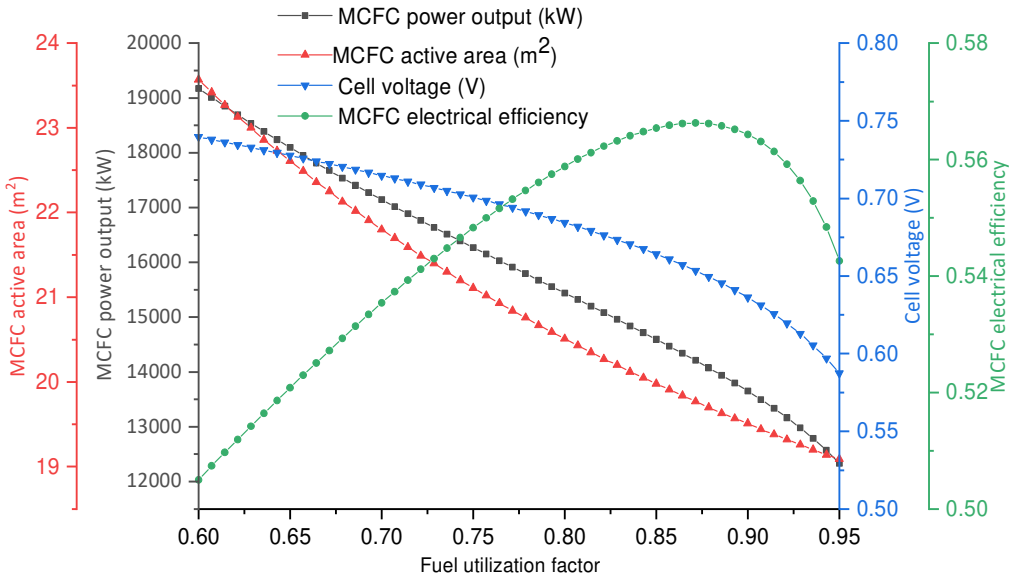

Fig. 7. Influence of the fuel utilization factor on fuel cell power output, active area, voltage and its electrical efficiency

An analysis of the performance of the plant has been conducted with the change of U_F from 0.6 to 0.95 for assigned U_{CO2} (0.75) and current density (1100 A/m^2). Since the flow rate of exhaust gases from the gas turbine is constant, the increase of the U_F caused low fuel consumption at the anode side, as shown in Fig. 7. Moreover, increasing the U_F causes adverse effects on the cell voltage. The lower U_F not only means that the fuel is not utilized in the electrochemical reactions, but also a considerable energy loss in the fuel cell stack is experienced. As far as the MCFC power output is reduced due to cell voltage loss and decreases in fuel cell active area with higher U_F, the fuel consumption rate at the anode side will decrease by increasing the U_F. Consequently, the electrical efficiency of the fuel cell will be increased by increasing the U_F. The change of U_F has a significant effect on the flow rate of anode inlet mass instead of the output power of the fuel cell. Hence, the MCFC electrical efficiency increases firstly and decreases subsequently under the specified U_{CO2}.

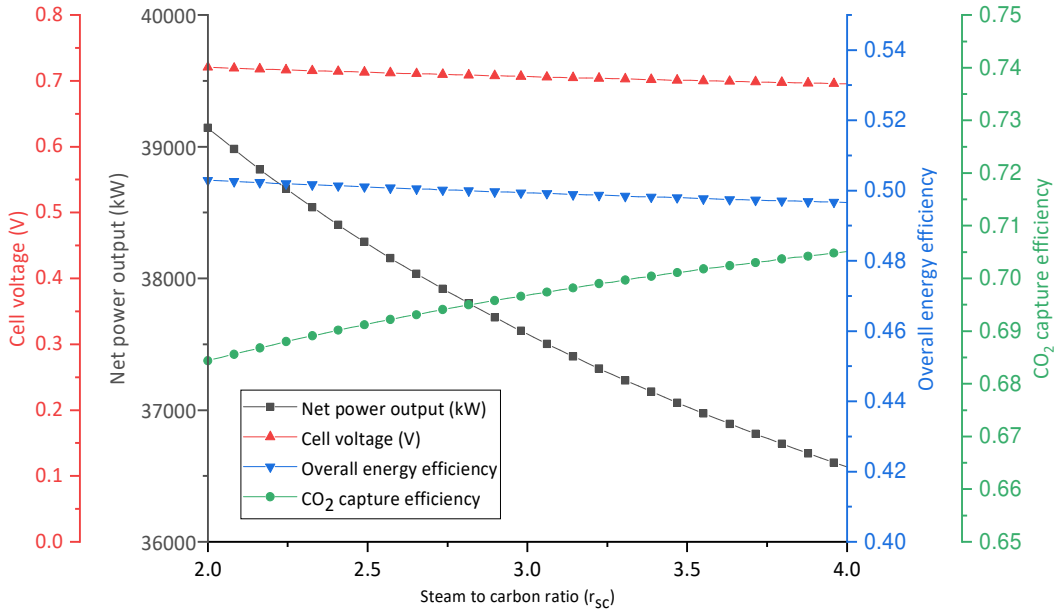

Fig. 8. Influence of the r_{SC} on net power output, fuel cell voltage, overall energy efficiency, CO_2 capture efficiency

As illustrated in Fig. 8, the variation of r_{SC} has straightforward effects on the overall energy efficiency and fuel cell voltage. Also, higher net power output is obtained by lower r_{SC}, but the variation of the r_{SC} does

not affect the overall efficiency significantly. In contrast, increasing the steam-to-carbon ratio will prepare the fuel cell to capture more carbon dioxide and increase the CO_2 capture efficiency.

The gas turbine inlet temperature is another parameter and according to Fig. 9, it can be seen that the gas turbine inlet temperature makes slight influences on the gas turbine section and overall plant energy efficiencies. With the given assumption in Table 1, the mass flow rate of biomass is constant. According to this condition, a higher temperature is imposed higher combustion chamber performance, and the efficiency improvement is predicted. Henceforward, the supplied air by the combustion chamber is decreased and the descending trend of energy efficiency can be seen. However, the minimal overall energy efficiency variation is obtained, and rising the related temperature does not affect power generation dramatically.

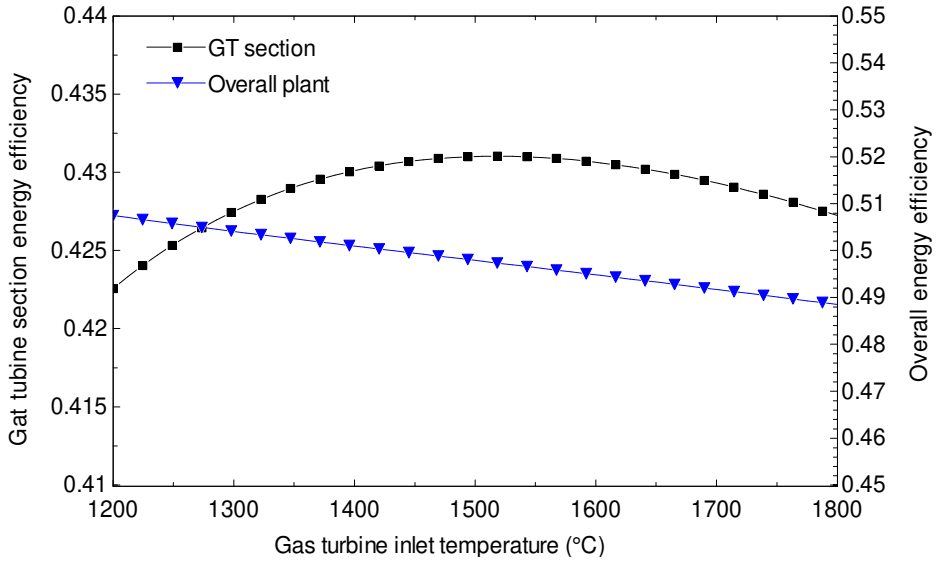

Fig. 9. Influence of the gas turbine inlet temperature on the gas turbine energy efficiency and overall plant energy efficiency

5.3. Comparative results

The outcomes of the simulations are compared between three plants which have already been introduced in Fig. 2a and Fig. 2b. To ensure to provide better comparison between them, the same simulation parameters are utilized based on Table 1. The distinctive characteristics results are listed in Table 4.

Table 4. Simulation results for the reference case and scenario 1 and 2 for power plant integration

	Reference case	Scenario 1	Scenario 2

		(Fig. 2a)	(Fig. 2b)
MSW mass flow rate, (ton/day)	300	300	300
GT electrical output (MW)	25.820	30.722	27.702
MCFC U_F/U_{CO2}, (%)	-	75/75	75/75
MCFC voltage, (V)	-	0.701	0.730
MCFC active area (m^2)	-	21.11	24.70
MCFC electrical output, (MW)	-	16.272	19.831
MCFC fuel mass flow rate, (kg/s)	-	0.593	0.694+0.336*
ORC turbine electrical output, (MW)	-	4.696	-
ST electrical output, (MW)	-	-	8.443
Power supply by cryogenic unit, (MW)	-	2.984	3.492
Total power output, (MW)	16.260	36.853	42.077
Overall energy efficiency, (%)	36.38	49.56	43.73
Carbon capture rate, (%)	N/A	70.14	70.13
Specific CO_2 emission, (kg_{CO2}/MW_eh)	854.9	146.9	158.7

* This value is sum of the fuel consumption by anode and additional combustion unit belong to the cathode side

Since constant biomass mass flow is assumed for all three predicted states, the results are compared based on the same fuel flow rate. The electricity generated by the reference case equals 25.82 MW, and its overall energy efficiency is 36.38 %. By integration of MCFC, we will have a significant increase in power generation capacity (16.272 MW in scenario 1 and 19.83 MW in scenario 2). WtE technology is also used to maximize the heat recovery in both scenarios and orc unit generates 4.696 MW power in scenario 1 and 8.443 MW power is produced by the steam turbine in the second scenario. Although a less portion of the power capacity is devoted to CO_2 capture in the cryogenic unit in the two predicted scenarios, the net power production in scenario 1 is 20.594 and in scenario 2 is 25.818 MW-point more than the reference case. Moreover, scenario 1 performs better than the scenario 2 from the energy efficiency point of view (49.56 % efficiency vs. 43.37 % efficiency). As reported in Table 4, the lowest increase in overall energy efficiency due to proposed integrations is 19.92%, which occurs in scenario 2. It is also noticeable that in scenario 1, 26.60 % growth in overall energy efficiency is obtained which reparents a better thermodynamic arrangement.

On the other hand, CO_2 separation (by MCFC) and removal (by cryogenic unit) efficiency for both scenarios (1 & 2) is almost identical and equal to around 70%. Specific CO_2 emission is another parameter which is reported in Table 4. This parameter indicates the amount of CO_2 emission per 1 MWh electrical energy production. This parameter is 146.4 (kg_{CO2}/MW_eh) for scenario 1, which is 82.3% lower than the reference case.

5.4.Exergy and Exergoeconomic results

The most relevant parameters associated with the exergy and exergoeconomic performances of proposed system components are outlined for scenario 1 and 2 in Table 6 and Table 7 respectively (Appendix B**:** Exergy and exergoeconomic analysis results for all streams in Scenario 1 and 2). In order to study the exergy and exergoeconomic defined by Equations (36) and (37), it is necessary to calculate the fuel and product values for the exergy and the exergy unit cost associated with each component of the system. To identify the most critical components, it is first necessary to rank them based on values of the summation of cost of exergy destruction and investment cost rates; then, the relative cost difference and the exergoeconomic factors will provide insights on the possible actions to undertake in order to improve the economic efficiency of the whole system.

By considering the exergoeconomic indicator, MCFC component results to have the highest value (87.29% in scenario 1 and 82.45% in scenario 2), instead the relative cost difference is extremely low, resulting in a small increase in the cost of the product with respect to the unit exergy cost of the fuel. After MCFC and air preheater, there is a group of components that totalize a $\dot{C_{des}} + \dot{Z}$ in the range of 0.001 and 0.085 USD/s in both scenarios. Most of components have low value of r_k, but the CO_2 cooler condenser reaches a value of 97.25% for the relative cost difference in both scenarios. This means that the CO_2 cooler condenser exergy unit cost is increased 97.25 times with respect to the cost of the fuels. This increase of product cost is imputed to inefficiencies and investment costs. Exergoeconomic factor is mostly used to select the strategy to perform the design evaluation of a selected plant, but in general gives information about the balance between inefficiencies and investment cost in a component. For mixers, since f_k tends to 0, the major cause of the cost increase has to be attributed to inefficiencies. Also, the ratio of exergy destruction for each system component is depicted in Fig. 10. The major responsibility of exergy destruction results to be the air preheater (21%), gasifier (16%), and combustion chamber (15%) in scenario 1. These results are mainly attributable to the three sources of irreversibility as the high temperature difference, electrochemical reaction, and combustion, respectively. As depicted in Fig. 10 for scenario 2, Gasifier, HRSG, and cathode inlet re-combustion (irreversibility due to electrochemical reaction, high temperature difference, and combustion, respectively) are characterized by the largest portion of the exergy destruction rates, respectively of 14 %, 12%, and 11%.

453

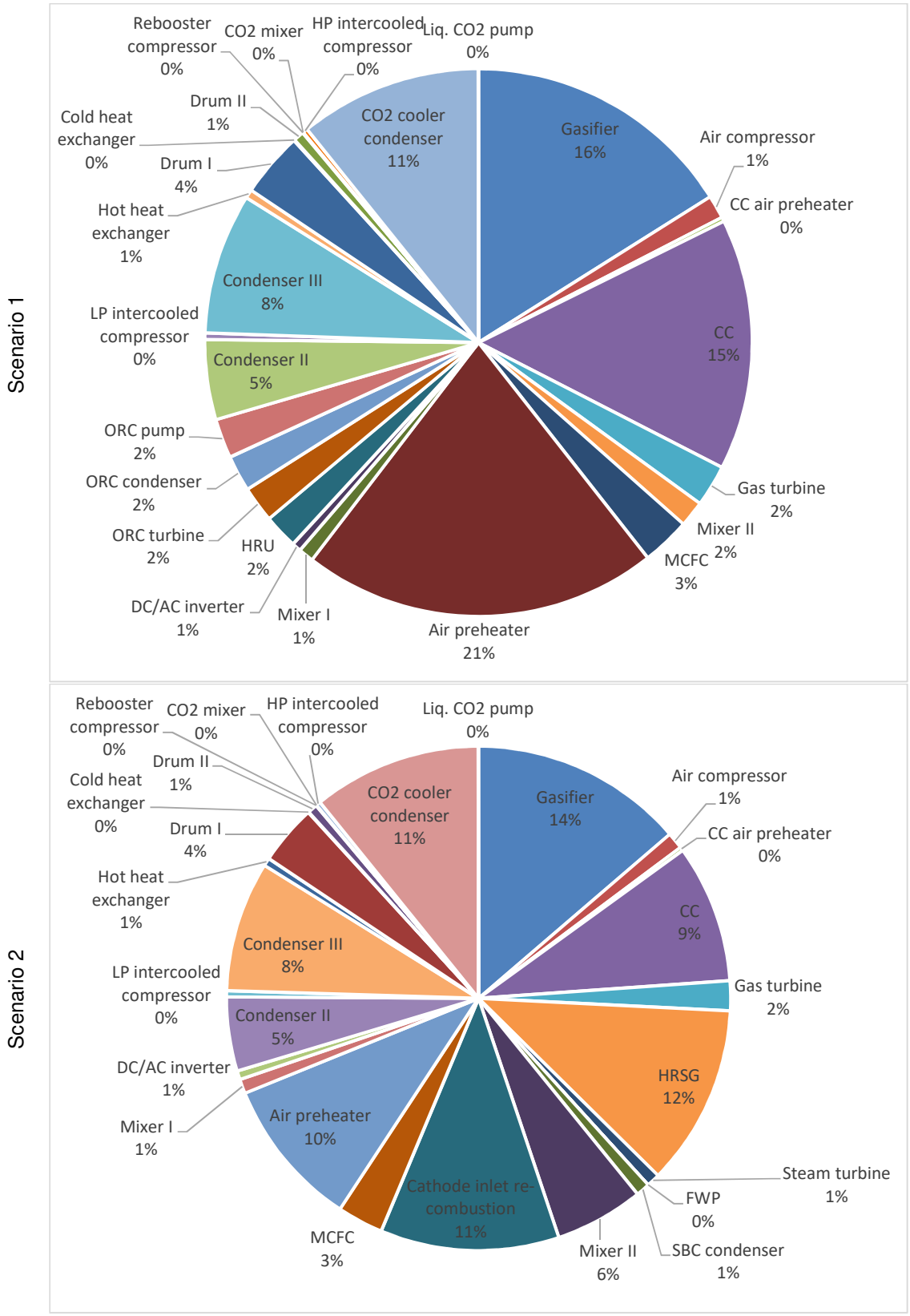
Scenario 1
Rebooster compressor 0%
CO2 mixer 0%
HP intercooled compressor 0%
Liq. CO2 pump 0%
Drum II 1%
Cold heat exchanger 0%
Drum I 4%
Hot heat exchanger 1%
CO2 cooler condenser 11%
Gasifier 16%
Air compressor 1%
CC air preheater 0%
Condenser III 8%
LP intercooled compressor 0%
Condenser II 5%
CC 15%
ORC pump 2%
ORC condenser 2%
ORC turbine 2%
HRU 2%
DC/AC inverter 1%
Mixer I 1%
Air preheater 21%
MCFC 3%
Mixer II 2%
Gas turbine 2%
Scenario 2
Rebooster compressor 0%
CO2 mixer 0%
HP intercooled compressor 0%
Liq. CO2 pump 0%
Drum II 1%
Cold heat exchanger 0%
Drum I 4%
Hot heat exchanger 1%
CO2 cooler condenser 11%
Gasifier 14%
Air compressor 1%
CC air preheater 0%
Condenser III 8%
LP intercooled compressor 0%
Condenser II 5%
CC 9%
Gas turbine 2%
DC/AC inverter 1%
Mixer I 1%
Air preheater 10%
HRSG 12%
Steam turbine 1%
FWP 0%
SBC condenser 1%
Cathode inlet re-combustion 11%
MCFC 3%
Mixer II 6%

Fig. 10. Exergy destruction percentage in different components of the proposed scenarios

6. Conclusions

This paper proposes a novel BECCS concept for power production, developed by integrating a downdraft gasifier, a directly fired gas turbine, MCFC, WtE technologies, and cryogenic CO_2 capture unit. ORC (in scenario 1) and SBC (in scenario 2) are considered as WtE technologies, and different arrangements are proposed for scenarios, based on the operative conditions and system's performance. Besides the definition and validation of the thermodynamic model, the proposed system has analyzed based on exergy and exergoeconomic analyses. the electric power generated in both scenarios has increased compared to the baseline state (16.272 MW in scenario 1 and 19.83 MW in scenario 2 compared to the reference case). While in scenario 1, only 0.6 kg/s of natural gas was added to the system as fuel for more power production, and the total amount of 1.03 kg/s natural gas was needed in scenario 2. Therefore, in terms of excessive consumption of natural gas fuel, scenario 1 is preferable compared to scenario 2 (due to avoiding the use of more fossil fuels, which was one of the objectives of the present study).

On the other hand, the overall exergy efficiency for the three developed cases is 30.63%, 43.95%, and 39.51% for the reference case, scenario 1, and scenario 2, respectively. Consequently, the best thermodynamic performance is devoted to scenario 1. The specific CO2 emission is another parameter that measures carbon dioxide emissions. The calculated results for three proposed scenarios based on Table 4 are equal to 854.9, 146.9, and 158.7 (kg_{CO2}/MW_eh). According to evidence, scenario 1 with 146.9 (kg_{CO2}/MW_eh) specific CO_2 emission is much better compared to the reference case and scenario 2.

Under the same current assumptions, the amount of 83.86 (USD/MW_eh) was obtained for LCOE in scenario 1 that is 55.76 (USD/MW_eh) more than the reference case and 3.55 (USD/MW_eh) less than the scenario 2.

Further developments will focus on the optimization of design parameters and provide conceptual design for the best option.

7. Acknowledgement

This work has been performed at SESAM group within the department of Energy, Politecnico di Milano.

Authors wish to thank Prof. Paolo Chiesa for his valuable guidance in the process of plant modeling.

8. Nomenclature

Abbreviations

AC	Air Compressor
Act	Activation
CC	Combustion Chamber
Cond	Condenser
FC	Fuel
GT	Gas Turbine
HEX	Heat Exchanger
HRU	Heat recovery Unit
HRSG	Heat Recovery Steam Generator
LCOE	Levelized Cost of Electricity
LHV	Lower Heating Value
MCFC	Molten Carbonate Fuel Cell
ORC	Organic Rankine cycle
Turb	Turbine
SBC	Steam bottoming cycle
ST	Steam Turbine

Mathematical symbols

A	Area
Ex	Exergy [kJ/kmol]
$\dot{C}$	Cost rate [$/h]
c	Unit cost of exergy rate [$/GJ]
J	Current desity [A/m^2]
$\dot{m}$	Mass flow rate [kg/s]
U_f	Fuel utilization factor
U_{O2}	Oxygen utilization factor
U_{CO2}	CO_2 utilization factor
r_P	Pressure ratio
r_{SC}	Steam to Carbon Ratio

Greek symbols

η	Efficiency [%]
ε	Effectiveness

9. Appendix A: Investment cost functions for components

Table 5
The cost functions of the various components in the proposed plant

Plant component	Capital cost function
Downdraft gasifier	$Z_{DDG} = c_0 \dot{m}_{biomas}^{0.67}$; $c_0 = 1600$ kg/hr

Compressors

$$Z_{AC} = \frac{c_{11} * \dot{m}_{in}}{c_{12} - \eta_{AC}} \left(\frac{P_{out}}{P_{in}}\right) ln\left(\frac{P_{out}}{P_{in}}\right)$$

$$c_{11} = 75 \frac{\$}{kg/s}; c_{12} = 0.9$$

Air preheaters

$$Z_{AP} = 4122 \left[\frac{Q_{AP}}{U_{AP} \Delta T_{LMTD,AP}}\right]; U_{AP} = 0.018$$

Combustion chambers

$$Z_{CC} = c_{21} \dot{m}_{air} \left(1 + \exp\left(c_{22} T_{cc,out} - c_{23}\right)\right) \left[\frac{1}{0.995 - \frac{P_{out,cc}}{P_{in,cc}}}\right]$$

$$c_{21} = 48.64 \frac{\$}{kg/s}; c_{22} = 0.018; c_{23} = 26.4$$

Gas turbine

$$Z_{GT} = \dot{W}_{GT} \left(1318.5 - 98.328 \ln\left(\dot{W}_{GT}\right)\right)$$

DC/AC inverter

$$Z_{DA,inv} = 10^5 \left(\frac{\dot{W}_{inv}}{500}\right)^{0.7}$$

MCFC

$$Z_{MCFC} = 2600\ \dot{W}_{FC,stack}$$

Heat Recovery Unit

$$Z_{HRU} = 390\ A_{HRU}^{0.78}$$

ORC turbine

$$Z_{ORCT} = 4750\ \dot{W}_{ORCT}^{0.75}$$

ORC pump

$$Z_{ORCP} = 1870\ \dot{W}_{ORCP}^{0.71}$$

ORC condenser

$$Z_{ORC,cond} = 1773\ \dot{m}_{air}$$

HRSG

$$Z_{HRSG} = Z_{EC} + Z_{EV} + Z_{SH}$$

$$Z_{EC} = 4131.8 \left(\mathrm{f_{P_{EC}}}\ \mathrm{f_{steam_{EC}}}\ \mathrm{f_{gas_{EC}}}\ \mathrm{K_{EC}^{0.8}}\right) + 13380\ \mathrm{f_{P_{EC}}}\ \dot{\mathrm{m}}_{\mathrm{steam}} + 1489.7\ \dot{\mathrm{m}}_{\mathrm{gas}}^{1.2}$$

$$\mathrm{f_{P_{EC}}} = 0.0971 \left(\frac{\left(\frac{P_{in,vapor}}{101.3}\right)}{30}\right) + 0.9029$$

$$\mathrm{f_{steam_{EC}}} = 1 + \exp\left(\frac{\left(\mathrm{T}_{sat,water} - 830\right)}{500}\right)$$

$$\mathrm{f_{gas_{EC}}} = 1 + \exp\left(\frac{\left(\mathrm{T_{out,gas}} - 990\right)}{500}\right)$$

$$K_{EC} = \left(\frac{\mathrm{Q_{EC}}}{\mathrm{DELTAT_{LMTD,EC}}}\right)$$

$$Z_{EV} = 4131.8 \left(\mathrm{f_{P_{EV}}}\ \mathrm{f_{steam_{EV}}}\ \mathrm{f_{gas_{EV}}}\ \mathrm{K_{EV}^{0.8}}\right) + 13380\ \mathrm{f_{P_{EV}}}\ \dot{\mathrm{m}}_{\mathrm{steam}} + 1489.7 \dot{\mathrm{m}}_{\mathrm{gas}}^{1.2}$$

$$f_{P_{EV}} = 0.0971\left(\frac{\left(\frac{P_{in,vapor}}{101.3}\right)}{30}\right) + 0.9029$$

$$f_{steam_{EV}} = 1 + \exp\left(\frac{\left(T_{sat,water} - 830\right)}{500}\right)$$

$$f_{gas_{EV}} = 1 + \exp\left(\frac{\left(T_{out,gas} - 990\right)}{500}\right)$$

$$K_{EV} = \left(\frac{Q_{EV}}{\Delta T_{LMTD,EV}}\right)$$

$$Z_{SH} = 4131.8\left(f_{P_{SH}}\, f_{steam_{SH}}\, f_{gas_{SH}}\, K_{SH}^{0.8}\right) + 13380\, f_{P_{SH}}\, \dot{m}_{steam} + 1489.7\dot{m}_{gas}^{1.2}$$

$$f_{P_{SH}} = 0.0971\left(\frac{\left(\frac{P_{in,vapor}}{101.3}\right)}{30}\right) + 0.9029$$

$$f_{steam_{SH}} = 1 + \exp\left(\frac{\left(T_{sat,water} - 830\right)}{500}\right)$$

$$f_{gas_{SH}} = 1 + \exp\left(\frac{\left(T_{out,gas} - 990\right)}{500}\right)$$

$$K_{SH} = \left(\frac{Q_{SH}}{\Delta T_{LMTD,SH}}\right)$$

Steam turbine	$Z_{ST} = 3880.5\, P_{ST}^{0.7}\left(1 + 3\frac{0.05}{1-\eta_{ST}}\right)\left(1 + 5\exp\left(\frac{T_{in,ST} - 866}{10.42}\right)\right)$
SBC condenser	$Z_{SBC,cond} = 280.74\left(\frac{Q_{SBC,cond}}{2200\, \Delta T_{LMTD}}\right)$
Feed Water Pump	$Z_{FWP} = 442\dot{W}_{FWP}^{0.71}\left(1 + \frac{0.2}{1-\eta_P}\right)$
Air condenser	$Z_{cond\ I} = 1773\, \dot{m}_{air}$
Hot heat exchanger	$Z_{HHE} = 3\, Z_{HHE_i}$ $Z_{HHE_i} = 4122\left[\frac{Q_{HHE_i}}{U_{HHE_i}\Delta T_{LMTD,HHE_i}}\right]; U_{HHE_i} = 0.018$
Drum	$Z_{KND} = 145315\left(\dot{m}_{CO_2,liq}\right)^{0.7}$
Cold heat exchanger	$Z_{CHE} = 4\, Z_{CHE_i}$ $Z_{CHE_i} = 4122\left[\frac{Q_{CHE_i}}{U_{CHE_i}\Delta T_{LMTD,CHE_i}}\right]; U_{CHE_i} = 0.018$

10. Appendix B: Exergy and exergoeconomic analysis results for all streams in Scenario 1 and 2

Table 6
Exergy and exergoeconomic analysis results of each system component for scenario 1

Component	$\dot{E}x_F$ (MW)	$\dot{E}x_P$ (MW)	$c_{F,k}$ ($ GJ^{-1})	$c_{P,k}$ ($ GJ^{-1})	$\dot{C}_{des_k}+\dot{Z}_k$ ($/s)	f_k (%)	r_k (-)
Gasifier	53.26	43.64	2.05	2.64	0.0258	23.49	22.37
Air compressor	11.51	10.68	23.30	26.00	0.0288	33.2	10.39
CC air preheater	1.63	1.47	27.09	31.59	0.0067	36.35	14.26
CC	63.24	54.35	11.71	14.69	0.1620	35.73	20.28
Gas turbine	54.35	52.87	14.69	16.30	0.0851	74.48	9.87
Mixer II	79.94	79.01	28.21	28.54	0.0261	0.00	1.16
MCFC	135.26	133.56	24.61	27.09	0.3304	87.29	9.13
Air preheater	70.38	57.79	27.09	33.39	0.3641	6.30	18.87
Mixer I	56.80	56.25	18.92	19.10	0.0104	0.00	0.97
DC/AC inverter	16.27	15.95	27.09	28.12	0.0158	46.61	3.68
HRU	7.45	6.24	27.09	32.56	0.0342	3.76	16.82
ORC turbine	9.90	8.63	32.37	39.29	0.0597	30.78	17.61
ORC condenser	1.97	0.57	9.45	33.87	0.0140	5.81	72.03
ORC pump	3.70	3.67	31.53	32.04	0.0020	42.88	1.59
Condenser II	3.77	0.97	6.02	27.09	0.0178	4.54	77.78
LP intercooled compressor	11.71	11.47	14.01	14.13	0.0041	28.48	0.87
Condenser III	5.20	0.21	1.59	27.52	0.0104	24.21	94.22
Hot heat exchanger	0.54	0.23	37.78	117.30	0.0264	55.83	67.78
Drum I	11.31	9.03	29.37	37.17	0.0703	4.46	20.97
Cold heat exchanger	0.13	0.094	40.46	100.50	0.0053	75.94	59.75
Drum II	8.01	7.63	38.16	40.46	0.0176	17.89	5.64
Rebooster compressor	0.1	0.07	38.51	60.70	0.0016	37.35	36.56
CO_2 mixer	0.85	0.85	37.84	37.87	0.0001	0.00	0.10
HP intercooled compressor	1.71	1.56	18.23	19.49	0.0034	11.14	6.48
CO_2 cooler condenser	6.62	0.18	0.98	35.41	0.0064	9.21	97.25
Liq. CO_2 pump	1.34	1.33	34.98	35.46	0.0006	31.15	1.34

* This value is sum of the fuel consumption by anode and additional combustion unit belong to the cathode side

486

Table 7
Exergy and exergoeconomic analysis results of each system component for scenario 2

Component	$\dot{E}x_F$ (MW)	$\dot{E}x_P$ (MW)	$c_{F,k}$ ($ GJ^{-1})	$c_{P,k}$ ($ GJ^{-1})	$\dot{C}_{des_k}+\dot{Z}_k$ ($/s)	f_k (%)	r_k (-)
Gasifier	53.26	43.64	2.05	2.64	0.0259	23.49	22.37
Air compressor	10.40	9.65	24.28	27.06	0.0268	32.29	10.27
CC air	1.91	1.75	40.21	45.54	0.0093	29.88	11.7

preheater							
CC	55.04	48.85	8.26	10.6	0.1133	54.75	21.87
Gas turbine	48.85	47.52	10.6	12.14	0.0733	80.67	12.68
HRSG	18.21	10.12	10.6	19.48	0.0897	4.43	45.55
Steam turbine	10.14	9.54	19.48	20.73	0.0119	0.92	6.02
FWP	0.028	0.026	21.23	23.35	0.0001	26.3	9.11
SBC condenser	1.08	0.45	19.48	46.48	0.0122	0.01	58.06
Mixer II	28.74	24.76	55.1	63.95	0.2191	0.00	13.84
Cathode inlet re-combustion	50.88	42.87	44.77	53.16	0.3595	0.28	15.77
MCFC	108.70	106.63	36.22	40.21	0.4263	82.45	9.94
Air preheater	33.83	27.13	40.21	50.62	0.2823	4.58	20.56
Mixer I	66.48	65.83	24.94	25.18	0.0161	0.00	0.97
DC/AC inverter	19.83	19.43	40.21	41.49	0.0248	35.65	3.07
Condenser II	4.44	1.13	8.62	40.21	0.0285	0.01	78.57
LP intercooled compressor	25.86	25.61	19.86	20.11	0.0063	21.93	1.22
Condenser III	6.07	0.24	2.05	38.97	0.0149	19.86	94.74
Hot heat exchanger	0.64	0.27	52.44	134.7	0.0351	46.1	61.07
Drum I	13.24	10.56	40.95	51.66	0.1132	3.10	20.74
Cold heat exchanger	0.15	0.11	55.81	124.5	0.0065	68.24	55.16
Drum II	9.37	8.93	52.8	55.81	0.0268	13.06	5.39
Rebooster compressor	0.11	0.08	50.16	76.55	0.0022	31.4	34.48
CO_2 mixer	0.95	0.94	51.9	51.96	0.0001	0.00	0.10
HP intercooled compressor	3.32	3.13	22.55	24.08	0.0048	9.21	6.35
CO_2 cooler condenser	7.75	0.21	1.20	43.74	0.0092	0.01	97.25
Liq. CO_2 pump	1.57	1.55	43.06	43.60	0.0008	25.99	1.25

* This value is sum of the fuel consumption by anode and additional combustion unit belong to the cathode side

11. References

[1] International Energy Agency - IEA. World Energy Outlook 2019. Int Energy Agency 2019. https://doi.org/DOE/EIA-0383(2012) U.S.

[2] Edenhofer O, Pichs-Madruga R, Sokona Y, Farahani E, Kadner S, Seyboth K, et al. Climate Change 2014: Mitigation of Climate Change. Contribution of Working Group III to the Fifth Assessment Report of the Intergovernmental Panel on Climate Change. vol. IPCC. United Kingdom and New York, NY, USA: 2014. https://doi.org/10.1017/CBO9781107415416.

[3] SDSN & FEEM. Roadmap to 2050: A manual for nations to decarbonise by mid-century. 2019.

[4] Collins C. Beyond Coal: Phase-Out Policies in the EU and Implications for the United States – Climate Institute 2019.

[5] Oei P, Hermann H, Herpich P, Holtemöller O, Schult C. Coal phase-out in Germany – Implications and policies for affected regions. Energy 2020:117004. https://doi.org/10.1016/j.energy.2020.117004.

[6] Hales D. Renewables 2018 global status report. 2018th ed. 2018.

[7] Basu P. Biomass gasification, pyrolysis and torrefaction: practical design and theory. Academic press; 2018.

[8] Tauqir W, Zubair M, Nazir H. Parametric analysis of a steady state equilibrium-based biomass gasification model for syngas and biochar production and heat generation. Energy Convers Manag 2019;199:111954.

[9] Luz FC, Rocha MH, Lora EES, Venturini OJ, Andrade RV, Leme MMV, et al. Techno-economic analysis of municipal solid waste gasification for electricity generation in Brazil. Energy Convers Manag 2015;103:321–37.

[10] Mazaheri N, Akbarzadeh AH, Madadian E, Lefsrud M. Systematic review of research guidelines for numerical simulation of biomass gasification for bioenergy production. Energy Convers Manag

2019;183:671–88.

[11] Ong HC, Chen W-H, Singh Y, Gan YY, Chen C-Y, Show PL. A state-of-the-art review on thermochemical conversion of biomass for biofuel production: A TG-FTIR approach. Energy Convers Manag 2020;209:112634.

[12] Solarte-Toro JC, Chacón-Pérez Y, Cardona-Alzate CA. Evaluation of biogas and syngas as energy vectors for heat and power generation using lignocellulosic biomass as raw material. Electron J Biotechnol 2018;33:52–62. https://doi.org/10.1016/j.ejbt.2018.03.005.

[13] Arena U. Process and technological aspects of municipal solid waste gasification. A review. Waste Manag 2012;32:625–39. https://doi.org/10.1016/j.wasman.2011.09.025.

[14] Keshavarzian S, Rocco M V, Gardumi F, Colombo E. Practical approaches for applying thermoeconomic analysis to energy conversion systems: Benchmarking and comparative application. Energy Convers Manag 2017;150:532–44.

[15] Keshavarzian S, Gardumi F, Rocco M V, Colombo E. Off-Design modeling of natural gas combined cycle power plants: An order reduction by means of thermoeconomic input–output analysis. Entropy 2016;18:71.

[16] Ding G, He B, Cao Y, Wang C, Su L, Duan Z, et al. Process simulation and optimization of municipal solid waste fired power plant with oxygen/carbon dioxide combustion for near zero carbon dioxide emission. Energy Convers Manag 2018;157:157–68. https://doi.org/10.1016/j.enconman.2017.11.087.

[17] Carneiro MLNM, Gomes MSP. Energy, exergy, environmental and economic analysis of hybrid waste-to-energy plants. Energy Convers Manag 2019;179:397–417.

[18] Ledón YC, González P, Concha S, Zaror CA, Arteaga-Pérez LE. Exergoeconomic valuation of a waste-based integrated combined cycle (WICC) for heat and power production. Energy 2016;114:239–52.

[19] Indrawan N, Thapa S, Bhoi PR, Huhnke RL, Kumar A. Electricity power generation from co-gasification of municipal solid wastes and biomass: Generation and emission performance. Energy 2018;162:764–75.

[20] Bhattacharya A, Manna D, Paul B, Datta A. Biomass integrated gasification combined cycle power generation with supplementary biomass firing: Energy and exergy based performance analysis. Energy 2011;36:2599–610. https://doi.org/10.1016/j.energy.2011.01.054.

[21] Mondal P, Ghosh S. Biomass Gasification based Combined Cycle Plant for Small Scale Generation: Part A-Energetic, Environmental and Economic Analyses. IOP Conf. Ser. Mater. Sci. Eng., vol. 377, IOP Publishing; 2018, p. 12054.

[22] Mondal P, Ghosh S. Integrated Biomass Gasification Combined Cycle Plant for Small Scale Generation: Part B-Exergetic and Exergo-economic Analyses. IOP Conf. Ser. Mater. Sci. Eng., vol. 377, IOP Publishing; 2018, p. 12055.

[23] Vassilev S V, Vassileva CG. Extra CO2 capture and storage by carbonation of biomass ashes. Energy Convers Manag 2020;204:112331.

[24] Mamaghani AH, Najafi B, Shirazi A, Rinaldi F. 4E analysis and multi-objective optimization of an integrated MCFC (molten carbonate fuel cell) and ORC (organic Rankine cycle) system. Energy 2015;82:650–63.

[25] Carapellucci R, Di Battista D, Cipollone R. The retrofitting of a coal-fired subcritical steam power plant for carbon dioxide capture: A comparison between MCFC-based active systems and conventional MEA. Energy Convers Manag 2019;194:124–39.

[26] Marefati M, Mehrpooya M, Shafii MB. A hybrid molten carbonate fuel cell and parabolic trough solar collector, combined heating and power plant with carbon dioxide capturing process. Energy Convers Manag 2019;183:193–209.

[27] El-Emam RS, Dincer I. Energy and exergy analyses of a combined molten carbonate fuel cell–Gas turbine system. Int J Hydrogen Energy 2011;36:8927–35.

561 [28] Verda V, Nicolin F. Thermodynamic and economic optimization of a MCFC-based hybrid system
562 for the combined production of electricity and hydrogen. Int J Hydrogen Energy 2010;35:794–806.

563 [29] Campanari S, Chiesa P, Manzolini G, Bedogni S. Economic analysis of CO2 capture from natural
564 gas combined cycles using Molten Carbonate Fuel Cells. Appl Energy 2014;130:562–73.
565 https://doi.org/10.1016/j.apenergy.2014.04.011.

566 [30] Duan L, Zhu J, Yue L, Yang Y. Study on a gas-steam combined cycle system with CO2 capture by
567 integrating molten carbonate fuel cell. Energy 2014;74:417–27.

568 [31] Akrami E, Ameri M, Rocco M V, Sanvito FD, Colombo E. Thermodynamic and exergo-economic
569 analyses of an innovative semi self-feeding energy system synchronized with waste-to-energy
570 technology. Sustain Energy Technol Assessments 2020;40:100759.

571 [32] Nami H, Akrami E, Ranjbar F. Hydrogen production using the waste heat of Benchmark
572 pressurized Molten carbonate fuel cell system via combination of organic Rankine cycle and
573 proton exchange membrane (PEM) electrolysis. Appl Therm Eng 2017;114:631–8.

574 [33] Nami H, Akrami E. Analysis of a gas turbine based hybrid system by utilizing energy, exergy and
575 exergoeconomic methodologies for steam, power and hydrogen production. Energy Convers
576 Manag 2017;143:326–37.

577 [34] Chiesa P, Campanari S, Manzolini G. CO2 cryogenic separation from combined cycles integrated
578 with molten carbonate fuel cells. Int J Hydrogen Energy 2011;36:10355–65.

579 [35] Bhoi PR, Huhnke RL, Kumar A, Indrawan N, Thapa S. Co-gasification of municipal solid waste
580 and biomass in a commercial scale downdraft gasifier. Energy 2018;163:513–8.

581 [36] Behzadi A, Gholamian E, Houshfar E, Habibollahzade A. Multi-objective optimization and
582 exergoeconomic analysis of waste heat recovery from Tehran's waste-to-energy plant integrated
583 with an ORC unit. Energy 2018;160:1055–68.

584 [37] Alhazmy MM, Najjar YSH. Augmentation of gas turbine performance using air coolers. Appl Therm

585 Eng 2004;24:415–29.

586 [38] Spinelli M, Campanari S, Consonni S, Romano MC, Kreutz T, Ghezel-Ayagh H, et al. Molten
587 Carbonate Fuel Cells for Retrofitting Postcombustion CO2 Capture in Coal and Natural Gas Power
588 Plants. J Electrochem Energy Convers Storage 2018;15:31001.

589 [39] Zhang J, Hu Q, Qu Y, Dai Y, He Y, Wang C-H, et al. Integrating food waste sorting system with
590 anaerobic digestion and gasification for hydrogen and methane co-production. Appl Energy
591 2020;257:113988.

592 [40] AlNouss A, McKay G, Al-Ansari T. A comparison of steam and oxygen fed biomass gasification
593 through a techno-economic-environmental study. Energy Convers Manag 2020;208:112612.

594 [41] Habibollahzade A, Gholamian E, Behzadi A. Multi-objective optimization and comparative
595 performance analysis of hybrid biomass-based solid oxide fuel cell/solid oxide electrolyzer cell/gas
596 turbine using different gasification agents. Appl Energy 2019;233:985–1002.

597 [42] Zainal ZA, Ali R, Lean CH, Seetharamu KN. Prediction of performance of a downdraft gasifier
598 using equilibrium modeling for different biomass materials. Energy Convers Manag 2001;42:1499–
599 515.

600 [43] Channiwala SA, Parikh PP. A unified correlation for estimating HHV of solid, liquid and gaseous
601 fuels. Fuel 2002;81:1051–63.

602 [44] Haghghi MA, Shamsaiee M, Holagh SG, Chitsaz A, Rosen MA. Thermodynamic, exergoeconomic,
603 and environmental evaluation of a new multi-generation system driven by a molten carbonate fuel
604 cell for production of cooling, heating, electricity, and freshwater. Energy Convers Manag
605 2019;199:112040.

606 [45] Vatani A, Khazaeli A, Roshandel R, Panjeshahi MH. Thermodynamic analysis of application of
607 organic Rankine cycle for heat recovery from an integrated DIR-MCFC with pre-reformer. Energy
608 Convers Manag 2013;67:197–207.

609 [46] Mamaghani AH, Najafi B, Shirazi A, Rinaldi F. Exergetic, economic, and environmental
610 evaluations and multi-objective optimization of a combined molten carbonate fuel cell-gas turbine
611 system. Appl Therm Eng 2015;77:1–11. https://doi.org/10.1016/j.applthermaleng.2014.12.016.

612 [47] Moran MJ, Bailey MB, Boettner DD, Shapiro HN. Fundamentals of engineering thermodynamics.
613 Wiley; 2018.

614 [48] Kotas TJ. The exergy method of thermal plant analysis. Elsevier; 2013.

615 [49] Rant Z. Energy value and pricing. Strojniški Vestnik-Journal Mech Eng 1955;1:4–7.

616 [50] Bejan A. Advanced Engineering Thermodynamics. John Wiley & Sons; 2006.

617 [51] Valero A, Usón S, Torres C, Valero A. Application of thermoeconomics to industrial ecology.
618 Entropy 2010;12:591–612.

619 [52] Lee YD, Ahn KY, Morosuk T, Tsatsaronis G. Exergetic and exergoeconomic evaluation of an
620 SOFC-Engine hybrid power generation system. Energy 2018.
621 https://doi.org/10.1016/j.energy.2017.12.102.

622 [53] Rocco M V., Colombo E, Sciubba E. Advances in exergy analysis: A novel assessment of the
623 Extended Exergy Accounting method. Appl Energy 2014.
624 https://doi.org/10.1016/j.apenergy.2013.08.080.

625 [54] Zare V. Exergoeconomic analysis with reliability and availability considerations of a nuclear
626 energy-based combined cycle power plant. Energy 2016;96:187–96.

627 [55] Ni M, Leung MKH, Leung DYC. Energy and exergy analysis of hydrogen production by a proton
628 exchange membrane (PEM) electrolyzer plant. Energy Convers Manag 2008;49:2748–56.
629 https://doi.org/10.1016/j.enconman.2008.03.018.

630 [56] Khani L, Mahmoudi SMS, Chitsaz A, Rosen MA. Energy and exergoeconomic evaluation of a new
631 power/cooling cogeneration system based on a solid oxide fuel cell. Energy 2016;94:64–77.

[57] Ameri M, Ahmadi P, Hamidi A. Energy, exergy and exergoeconomic analysis of a steam power plant: A case study. Int J Energy Res 2009;33:499–512.

[58] Campanari S, Chiesa P, Manzolini G. CO2 capture from combined cycles integrated with Molten Carbonate Fuel Cells. Int J Greenh Gas Control 2010;4:441–51. https://doi.org/10.1016/j.ijggc.2009.11.007.

[59] La Villetta M, Costa M, Massarotti N. Modelling approaches to biomass gasification: A review with emphasis on the stoichiometric method. Renew Sustain Energy Rev 2017;74:71–88.